nature biotechnology

Tandem fluorescent protein timers for *in vivo* analysis of protein dynamics

Anton Khmelinskii[1,2,7], Philipp J Keller[2,3,7], Anna Bartosik[1,2,8], Matthias Meurer[1,2,8], Joseph D Barry[4,8], Balca R Mardin[1], Andreas Kaufmann[2,6], Susanne Trautmann[2,5], Malte Wachsmuth[2], Gislene Pereira[5], Wolfgang Huber[4], Elmar Schiebel[1] & Michael Knop[1,2,5]

The functional state of a cell is largely determined by the spatiotemporal organization of its proteome. Technologies exist for measuring particular aspects of protein turnover and localization, but comprehensive analysis of protein dynamics across different scales is possible only by combining several methods. Here we describe tandem fluorescent protein timers (tFTs), fusions of two single-color fluorescent proteins that mature with different kinetics, which we use to analyze protein turnover and mobility in living cells. We fuse tFTs to proteins in yeast to study the longevity, segregation and inheritance of cellular components and the mobility of proteins between subcellular compartments; to measure protein degradation kinetics without the need for time-course measurements; and to conduct high-throughput screens for regulators of protein turnover. Our experiments reveal the stable nature and asymmetric inheritance of nuclear pore complexes and identify regulators of N-end rule–mediated protein degradation.

Systematic monitoring of proteome dynamics would require simultaneous measurement of protein turnover and subcellular trafficking at the single-cell and population scales. The importance of protein turnover was introduced in 1942 by Schönheimer, who noted that "all constituents of living matter, whether functional or structural, of simple or of complex constitution, are in a steady state of rapid flux"[1]. Protein homeostasis is now understood as a balance between protein synthesis, through transcription and translation, and protein degradation, through processes such as proteasomal and lysosomal degradation, tuned in response to intrinsic and extrinsic inputs. Alterations in protein turnover are observed in aging organisms and underlie various diseases. Deregulated degradation of cell cycle control proteins such as the p53 tumor suppressor plays a critical role in many forms of human cancers[2]. Abnormal trafficking and degradation of a mutant form of a chloride ion channel causes cystic fibrosis[3]. Moreover, accumulation of specific proteins is linked to neurodegenerative disorders such as Alzheimer's, Parkinson's and Huntington's diseases[4]. Therefore, understanding protein turnover and mobility could provide new strategies for targeted clinical interference to treat such diseases[5].

Although there are many ways to measure protein abundance in living cells, few techniques exist for systematically measuring protein turnover and trafficking down to subcellular resolution. Protein turnover is typically analyzed with pulse-chase metabolic labeling followed by immunoprecipitation, which measures the amount of a specific protein remaining after a short period of labeling. Metabolic labeling can be combined with mass spectrometry to determine the degradation kinetics of multiple proteins in parallel[6]. However, this technique does not allow monitoring of protein turnover in living cells. The rate of protein turnover in living cells can be measured by pulse-labeling fluorescent-protein fusion proteins through photoactivation or photobleaching and then measuring the change of fluorescent signal over time[7,8]. Turnover rates can also be determined with single time-point measurements by normalizing the abundance of fluorescent-protein fusions to a reference fluorescent protein expressed from the same mRNA, using global protein stability profiling[9] or a similar method[10]. This approach was applied to identify E3 ubiquitin-protein ligase substrates[11], but the use of a soluble reference hinders studies of subcellular protein dynamics. The most common method of studying subcellular trafficking is to selectively label fluorescent-protein fusion proteins with photoactivation or photobleaching and to follow them over time[12,13]. Biochemical approaches, such as cell fractionation followed by Western blot analysis, have also been used, but they are not applicable to living cells.

So-called 'fluorescent timer' proteins have the potential to report on both protein turnover and subcellular trafficking in living cells. A conventional fluorescent timer is a fluorescent protein that switches color over time as its fluorophore undergoes successive chemical reactions[14]. The ratio of fluorescence intensities of the second and first fluorescent states, or intensity ratio, provides a measure of protein age (**Fig. 1a**), which should enable the use of fluorescent protein timers to follow protein turnover and mobility. However, widespread application of fluorescent timers has so far been hampered either by their tendency to form oligomers[14–16], which can perturb the behavior of tagged proteins, or by their low brightness.

[1]Center for Molecular Biology of the University of Heidelberg (ZMBH), DKFZ-ZMBH Alliance, Heidelberg, Germany. [2]European Molecular Biology Laboratory (EMBL), Cell Biology and Biophysics Unit, Heidelberg, Germany. [3]Janelia Farm Research Campus, Howard Hughes Medical Institute, Ashburn, Virginia, USA. [4]European Molecular Biology Laboratory, Genome Biology Unit, Heidelberg, Germany. [5]German Cancer Research Center (DKFZ), DKFZ-ZMBH Alliance, Heidelberg, Germany. [6]Present address: ETH Zurich, Light Microscopy and Screening Center, Zurich, Switzerland. [7]These authors contributed equally to this work. [8]These authors provided equivalent support for this work. Correspondence should be addressed to M.K. (m.knop@zmbh.uni-heidelberg.de) or E.S. (e.schiebel@zmbh.uni-heidelberg.de).

Received 28 March; accepted 19 May; published online 24 June 2012; doi:10.1038/nbt.2281

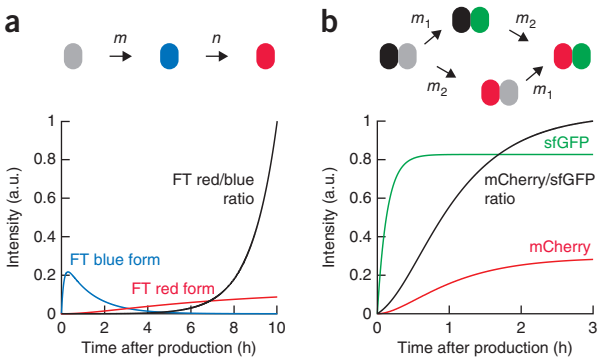

Figure 1 Tandem fluorescent protein fusions as fluorescent timers. (**a**) Illustration of a conventional fluorescent timer (FT) with maturation rate constants (*m*, *n*) of the fluorescent timer 'fast-FT'[15]. (**b**) Behavior of a tandem fusion of mCherry (black, red) and sfGFP (gray, green) with the maturation rate constants (m_1, m_2) determined in this study (**Supplementary Methods**). For simplicity, a one-step process represents mCherry maturation. Fluorescence intensity curves are normalized to the brightness of sfGFP. Ratios are normalized to the maximum in each plot.

Here we describe tandem fluorescent protein timers (tFTs) that overcome these limitations. The timers can be designed to measure time spans ranging from ~10 min to many hours. To demonstrate the versatility of this approach, we used tFTs to study subcellular trafficking of nuclear pore complexes and to identify regulators of protein degradation with high-throughput screens using data collected at a single time point.

RESULTS

Tandem fluorescent protein timers

We designed tFTs by fusing pairs of single-color fluorescent proteins having well-separated emission spectra (**Fig. 1b**). After translation, each protein becomes fluorescent with characteristic kinetics as it matures. A tandem fluorescent protein fusion can function as a fluorescent timer if the two fluorophores mature with different kinetics, whereby the ratio of fluorescence intensities from the two fluorescent protein domains is an indicator of the age of a pool of proteins (**Fig. 1b**). The broad range of readily available single-color fluorescent proteins may be exploited to quickly generate new fluorescent timers with properties distinct from conventional fluorescent timers (**Supplementary Note 1**). In particular, the maturation kinetics of the more slowly maturing fluorescent protein largely defines the useful time range of a tFT (**Supplementary Fig. 1**).

To demonstrate this approach, we combined the monomeric red fluorescent protein mCherry, which matures with a half-time of ~40 min[17], with a monomeric variant of the superfolder green fluorescent protein sfGFP, which becomes fluorescent within minutes of synthesis[18]. A pool of mCherry-sfGFP molecules should be mostly green-fluorescent shortly after synthesis and gradually acquire red fluorescence over time, such that the ratio of red to green fluorescence is a function of the age of the protein pool (**Fig. 1b**).

Dynamics of cellular components

To demonstrate the usefulness of tFTs, we fused mCherry-sfGFP to proteins with age-dependent subcellular localization in the budding yeast *S. cerevisiae* (Online Methods and **Supplementary Table 1**). First, we examined the inheritance of spindle pole bodies (SPBs). SPBs are the yeast equivalent of the centrosome and duplicate in a conservative manner. During mitosis the preexisting (old) SPB is segregated into the daughter cell (bud), whereas the new SPB is retained in the mother cell[19]. Accordingly, cells expressing the SPB marker Spc42-mCherry-sfGFP displayed a higher mCherry/sfGFP intensity ratio at the SPB in the bud (R_b) than at the SPB in the mother (R_m) (**Fig. 2a–c**). The R_b/R_m ratio decreased as the relative age difference between the two SPBs decreased with cell cycle progression (**Fig. 2b**). Deletion of the *KAR9* gene, which encodes a factor that mediates interactions between cytoplasmic microtubules and the bud cortex, impairs SPB inheritance such that the new SPB is segregated into the bud in ~40% of the cells[19]. Consistently, a corresponding fraction of *kar9*Δ cells showed R_b/R_m ratios below one (**Fig. 2c**).

In contrast to SPBs, preexisting pools of the integral plasma membrane proteins Hxt1 and Pma1 are retained in the mother compartment, whereas the bud receives newly synthesized polypeptides[20,21]. Accordingly, the mCherry/sfGFP intensity ratio *R* was higher at the plasma membrane in the mother cell than in the bud for both proteins tagged with mCherry-sfGFP (**Fig. 2d**, R_b/R_m ratio of 0.43 ± 0.07 and 0.37 ± 0.09 for Hxt1 and Pma1, respectively; mean ± s.d., $n = 40$).

Finally, we examined structures marked with Rax2. Rax2 appears at the cortex of emerging buds and relocalizes to the site of cell division (bud neck), where it forms stable rings associated with bud scars, which mark sites of previous cell divisions[22] (**Fig. 2e**). The mCherry/sfGFP intensity ratio of Rax2-mCherry-sfGFP correlated positively with the age of labeled structures (**Fig. 2f**). The intensity ratio was lower at emerging buds or bud necks than at bud scars. When measured at birth scars, the sites of the first cell division, the intensity ratio increased as cells progressed through successive cell cycles. Structures of four generations could be distinguished by their intensity ratio values in cells dividing for the third time (**Fig. 2f**). Together, these experiments demonstrate that the tandem mCherry-sfGFP fusion functions as a timer. Comparative measurements with this timer are robust within single cells as the relative age of different structures was determined accurately in nearly every individual cell (**Fig. 2**). However, significant cell-to-cell variation in absolute mCherry/sfGFP intensity ratios of similar structures is apparent (**Fig. 2f**). The stochastic nature of fluorescent protein maturation and distinct cell histories contribute to this variability (**Supplementary Note 2**).

Next, we applied the mCherry-sfGFP timer to analyze the mobility and inheritance of nuclear pore complex (NPC) components. Each NPC comprises ~30 different proteins, called nucleoporins, that form pores in the nuclear envelope and control nucleocytoplasmic transport and nuclear organization[23] (**Fig. 3a**). In organisms with open mitosis, NPCs disassemble when the nuclear envelope breaks down during cell division but are stable in nondividing cells. Stable NPCs can accumulate damage over time, which disrupts the nucleocytoplasmic permeability barrier in aging cells[24]. In contrast, *S. cerevisiae* undergoes closed mitosis, and its NPCs are also stable in dividing cells[25,26]. As cell division is inherently asymmetric in this organism[27], we used a library of strains expressing nucleoporins tagged with mCherry-sfGFP to investigate the possibility of age-dependent segregation of NPCs during yeast mitosis (Online Methods, **Supplementary Fig. 2** and **Supplementary Table 1**). Several nucleoporins, in particular scaffold NPC components, exhibited substantially higher mCherry/sfGFP intensity ratios at the nuclear envelope than in the cytoplasm (**Fig. 3b** and **Supplementary Fig. 3**). This result is consistent with the notion that the core of the NPC is stable and its nucleoporins are not exchanged with the cytoplasm (**Supplementary Note 3**), and it indicates that tFTs can inform on intracellular protein mobility.

Notably, the mCherry/sfGFP intensity ratio was higher at the nuclear envelope in the bud than in the mother for most nucleoporins (**Fig. 3c**; the R_b/R_m ratio varied with nucleoporin stability as expected;

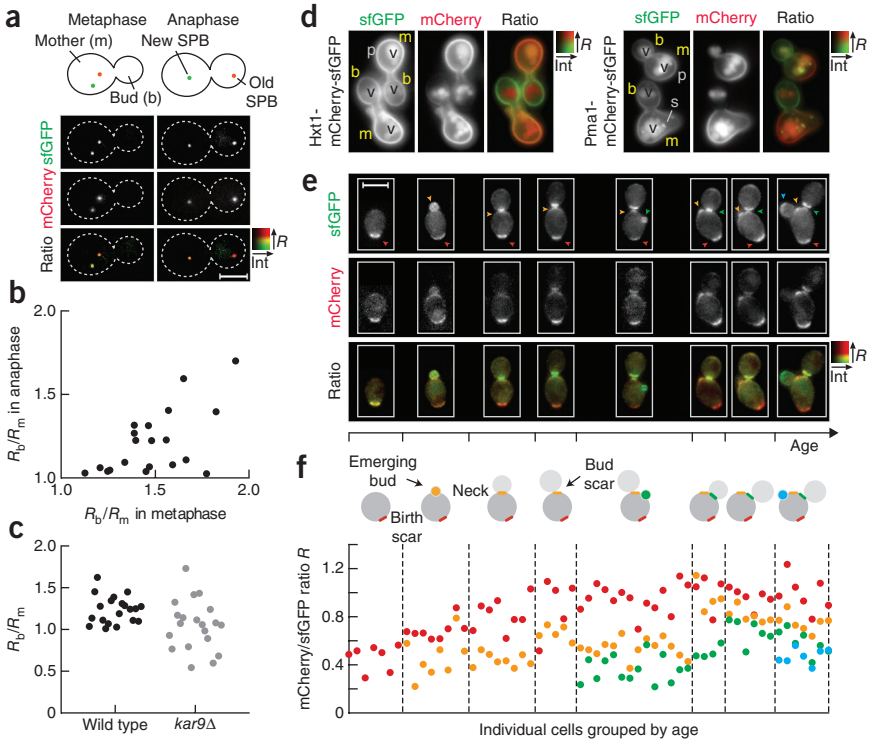

Figure 2 Analysis of differential inheritance of cellular structures with the mCherry-sfGFP timer. (**a**–**c**) mCherry/sfGFP intensity ratios of Spc42-mCherry-sfGFP at SPBs retained in the mother (R_m) and at SPBs directed toward or in the bud (R_b). (**a**) Ratiometric images (bottom panel) are color-coded according to sfGFP intensity (Int) and intensity ratio R, as indicated. Scale bar, 3 µm. (**b**) R_b/R_m ratios in cells from **a** followed with time-lapse microscopy. Each point corresponds to a single cell analyzed in metaphase (t = 0 min) and at the end of anaphase (t = 30 min). (**c**) R_b/R_m ratios in wild type and *kar9*Δ cells at the end of anaphase. (**d**) mCherry/sfGFP intensity ratios of Hxt1 and Pma1 fusions at the plasma membrane (p), vacuoles (v) and secretory compartments (s) in mother (m) and bud (b) cells. Ratiometric mCherry/sfGFP images are color-coded as indicated. Scale bar, 5 µm. (**e**,**f**) mCherry/sfGFP intensity ratios of structures marked with Rax2-mCherry-sfGFP. (**e**) Images of representative diploid cells ordered according to cell age and cell cycle stage. Different structures are marked with arrowheads according to origin (red, birth; orange, first cell cycle; green, second cell cycle; cyan, third cell cycle). Ratiometric mCherry/sfGFP images are color-coded as indicated. Scale bar, 5 µm. (**f**) Quantification of **e**. mCherry/sfGFP intensity ratios measured at the structures indicated in the cartoons are plotted for individual cells, grouped and ordered according to the age of the mother cell.

Supplementary Fig. 4). This indicates that NPCs are on average older in the bud than in the mother. Two mechanisms can account for the asymmetric distribution of NPC age: preferential assembly of new NPCs in the mother cell or biased segregation of old NPCs into the bud. We sought to distinguish between these two possibilities. As assembly of new NPCs is limited during anaphase[28,29], we directly examined the segregation of old NPCs using the nucleoporin Nup2 tagged with the red fluorescent protein DsRed1. DsRed1 undergoes extremely slow maturation, with a half-time of ~10 h[30], and thus Nup2-DsRed1 labels only the oldest NPCs (**Supplementary Fig. 5**).

Time-lapse imaging revealed Nup2-DsRed1 dots moving into the bud together with the nucleus, as the nuclear envelope was traversing the bud neck in early anaphase (**Fig. 3d** and **Supplementary Movie 1**). Individual Nup2-DsRed1 dots also moved from the mother to the bud in late anaphase when the two nuclei were connected by a thin tubule of nuclear envelope (**Fig. 3d** and **Supplementary Movie 2**), raising the possibility that old NPCs are actively transported into the bud. At the end of nuclear division, 50 ± 20% of Nup2-DsRed1 dots (mean ± s.d., n = 83 cells) were found in the bud. This result was independently confirmed with recombination-induced tag exchange[31] for differential labeling of old and new NPCs (**Supplementary Fig. 6a**,**b**). Taking into account that the bud receives only ~38% of all NPCs[29], equal partitioning of old NPCs between mother and bud nuclei results in a 1.53 ± 0.13 fold higher density of old NPCs in the bud (the difference between mother and bud NPC densities is statistically significant with $P < 10^{-6}$ in a paired t-test) (**Supplementary Fig. 6c**).

We conclude that asymmetric distribution of NPC age is achieved by age-dependent partitioning of existing NPCs between mother and bud nuclei. Preferential physical interaction between chromosomes and older or more mature NPCs could contribute to equal partitioning of such NPCs in the context of an overall asymmetric nuclear division. Because yeast mitosis leads to rejuvenation of the bud in terms of replicative life span[27], our results imply that old NPCs are not synonymous with damage, although a potential role of NPCs in yeast aging has been discussed[32]. Instead, age-dependent segregation of NPCs could ensure that the bud receives enough mature NPCs for competent nucleocytoplasmic transport and nuclear organization. Analysis of changes in NPC functionality over time will be required to test this hypothesis in the future. Taken together, our experiments show that tFTs can be used to study the relative age, segregation, mobility and inheritance of cellular components.

Snapshot analysis of protein stability

Because tFTs provide a readout of the average age of a protein, which is determined by its rate of turnover, tFTs also facilitate the study of the kinetics of protein turnover. Briefly, owing to the slow maturation of mCherry relative to sfGFP, the mCherry/sfGFP intensity ratio in steady state should decrease with the increasing degradation rate of mCherry-sfGFP fusions, independently of the rate of protein production (**Supplementary Note 4** and **Supplementary Theory**). Thus, it should be possible to infer degradation kinetics from a single time-point snapshot of fluorescence measurements. To demonstrate this, we engineered a series of constructs with different stabilities by varying the N-terminal residue of a degradation signal, the N-degron, fused to the N-terminus of mCherry-sfGFP. Each construct encoded a different pro-N-degron (the N-degron with a ubiquitin (Ubi) moiety at the N terminus) followed by mCherry-sfGFP (**Fig. 4a** and **Supplementary Table 2**). Upon translation, the N-terminal ubiquitin is removed, thereby exposing the N-degron. Constructs with destabilizing N-terminal residues are marked for degradation by the E3 ubiquitin-protein ligase Ubr1 as part of the N-end rule pathway of protein degradation[33].

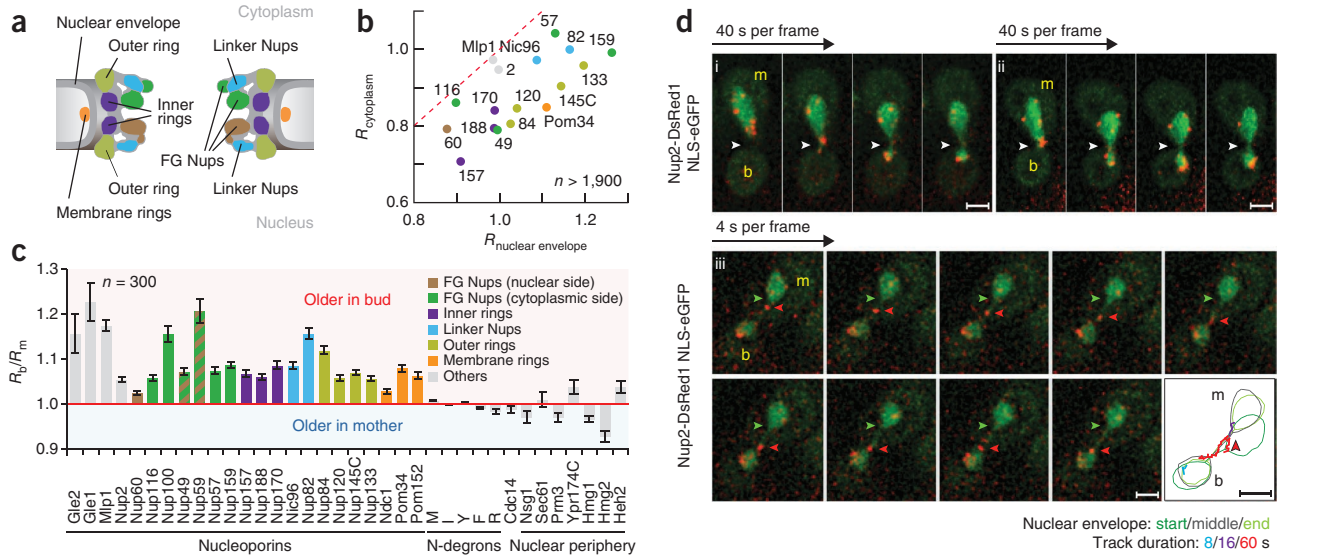

Figure 3 Inheritance of nuclear pore complexes during yeast mitosis. (**a**) Relative position of different structural elements of the NPC, according to reference 46. (**b**) Comparison of mCherry/sfGFP intensity ratios (R) of the indicated nucleoporins (e.g., Nup60 abbreviated as 60) at the nuclear envelope and in the cytoplasm. Colors indicate the structural assignments according to **a**. Intensity ratios at the red dashed line are equal in the two compartments. Error bars (s.e.m.) are smaller than the symbols representing the data points. (**c**) mCherry/sfGFP intensity ratios of the indicated proteins fused to mCherry-sfGFP were measured in mother (R_m) and bud (R_b) compartments at the nuclear envelope (nucleoporins, nuclear periphery proteins), in the nucleolus (Cdc14) or in the cytoplasm. Symmetrically localized nucleoporins with phenylalanine-glycine (FG) repeats (FG Nups) are colored in green/brown. Error bars indicate s.e.m. The difference between R_m and R_b is significant for all nucleoporins ($P < 0.006$ in an unpaired t-test) except Gle2 ($P > 0.01$). (**d**) (i,ii) Movement of Nup2-DsRed1 dots in early anaphase relative to the bud neck (white arrowheads). (iii) A single Nup2-DsRed1 dot (red arrowheads) moves from the base of the mother nucleus (green arrowheads) into the bud. Tracks of NPC movement are color coded according to duration; tracking stopped when the NPCs moved out of focus; arrowhead indicates initial direction of movement. Mother (m) and bud (b) compartments are indicated. Scale bars, 2 μm.

Single time-point fluorescence measurements with flow cytometry showed that the mCherry/sfGFP intensity ratios of yeast strains expressing different constructs increased as a function of construct stability (**Fig. 4b**). Inhibition of degradation by deletion of *UBR1* led to similar intensity ratios for all constructs, whereas overexpression of *UBR1* decreased the intensity ratio of unstable constructs (**Fig. 4b**). Moreover, the intensity ratio was independent of the protein production rate, as demonstrated with single-cell analysis of a strain with heterogeneous protein expression levels caused by plasmid copy number variations (**Fig. 4c**) or by using promoters of different strengths (**Fig. 4d**). These results demonstrate that the mCherry/sfGFP intensity ratio provides a direct readout of protein degradation kinetics in steady state, in agreement with the mathematical description of mCherry-sfGFP turnover (**Supplementary Note 4** and **Supplementary Theory**). Ratiometric measurements of constructs with the 20 possible N-terminal residues demonstrate the sensitivity of this approach (**Supplementary Fig. 7**).

According to our experimental estimates of mCherry and sfGFP maturation kinetics (**Supplementary Methods** and **Supplementary Fig. 8a**), the mCherry-sfGFP timer should be suitable to study the degradation of proteins with half-lives between ~10 min and ~8 h (**Supplementary Fig. 8b,c**). As the *S. cerevisiae* proteome has an average half-life of ~43 min[34], the majority of proteins could be systematically investigated with this tFT. However, potential artifacts caused by tagging should be considered (**Supplementary Note 5**). In human cells, proteins appear to be more stable, with an average half-life of ~10 h[7]. tFTs with red fluorescent proteins that mature more slowly than mCherry, with a time range shifted toward reduced turnover (**Supplementary Figs. 1** and **9**), should be more appropriate for such

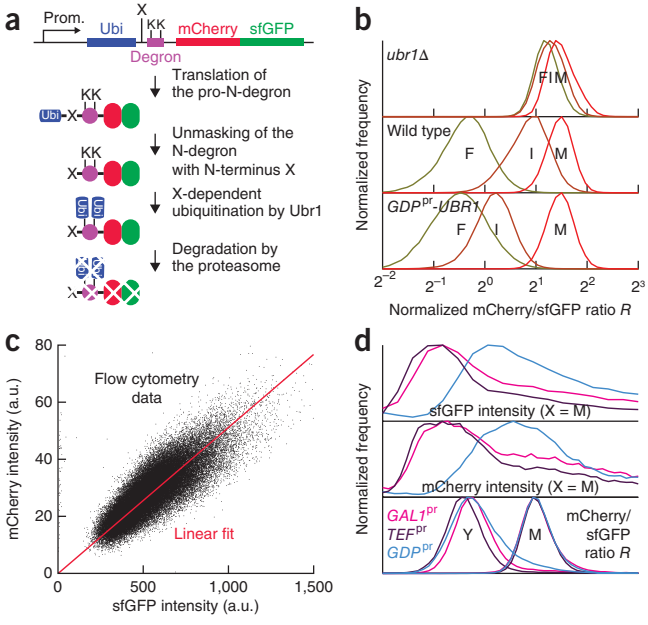

Figure 4 Analysis of protein turnover with the mCherry-sfGFP tFT. (**a**) Scheme of Ubi-X-mCherry-sfGFP constructs. N-degron stability depends on the amino acid residue X in the pro-N-degron, such that X = M (stable) > I > Y > F (unstable). (**b**) Ratiometric fluorescence measurements of Ubi-X-mCherry-sfGFP constructs with the indicated amino acid residues X in wild type, *ubr1*Δ and *GDP*^{pr}*-UBR1* (overexpression of *UBR1*) strains. (**c**) sfGFP and mCherry intensities of single cells expressing Ubi-M-mCherry-sfGFP. (**d**) sfGFP and mCherry intensities (top two panels) and mCherry/sfGFP intensity ratios (bottom panel) of cells expressing the indicated Ubi-X-mCherry-sfGFP fusions from *GAL1*, *TEF* and *GDP* promoters.

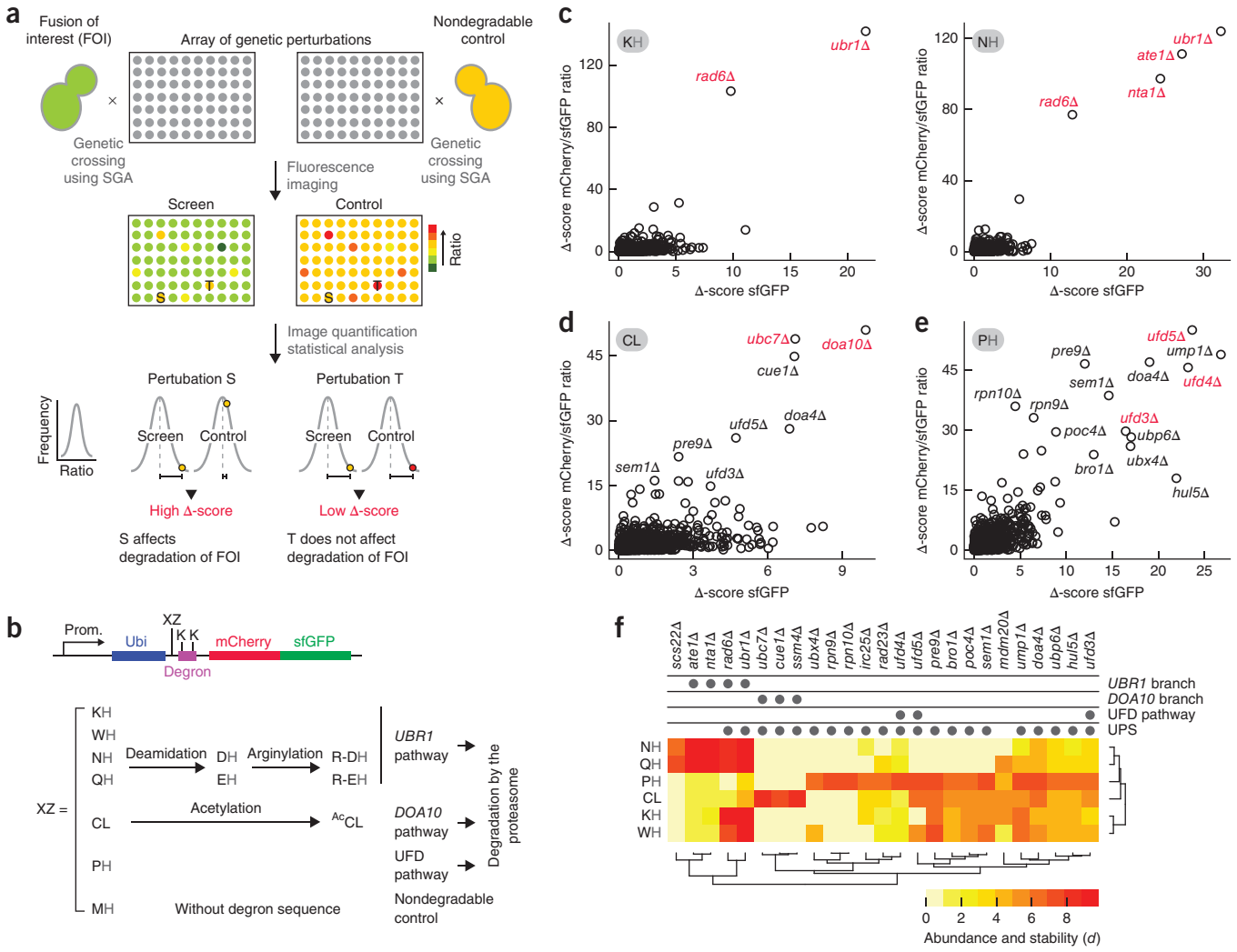

Figure 5 Identification of components of the N-end rule pathway. (**a**) High-throughput pipeline for systematic identification of regulators of protein turnover. The analysis of mCherry/sfGFP intensity ratios is exemplified for two genetic perturbations (S, T). (**b**) N-degrons used to screen for components of the N-end rule pathway. The two N-terminal amino acid residues define the N-degron recognized by Doa10 (residues XZ in the pro-N-degron). (**c**–**e**) Identification of gene deletions that stabilize the indicated N-degrons. Only gene deletions with positive Δ-scores are shown. Expected hits are highlighted in red. (**f**) Heat map of top gene deletions that increase the abundance and stability of each N-degron. The impact of each gene deletion is represented by a single color-coded value (*d*), which combines the Δ-scores of the sfGFP and mCherry/sfGFP channels (Online Methods). Gene deletion strains with $d \geq 6$ in at least one screen replicate were included in the heat map. Mutants of the ubiquitin-proteasome system (UPS) are indicated.

cases. Nevertheless, the time range of mCherry-sfGFP was sufficient to evaluate the turnover of different fusions expressed in HeLa cells (**Supplementary Fig. 10**).

High-throughput screening for regulators of protein turnover

Despite recent advances, identifying factors responsible for degradation of specific proteins is challenging[7–10]. We developed a high-throughput assay based on tFTs to screen for regulators of protein turnover in *S. cerevisiae* (**Fig. 5a**). We applied this approach to identify components of the N-end rule pathway of protein degradation. The mCherry-sfGFP timer was fused to five pro-N-degrons, each composed of Ubi followed by an N-degron with a destabilizing motif for a specific branch of the N-end rule pathway. Constructs with lysine, tryptophan, asparagine or glutamine as the N-terminal residue of the N-degron (Ubi-K/W/N/Q-mCherry-sfGFP) are marked for degradation by Ubr1 in combination with the E2 enzyme Rad6. The construct with a cysteine-leucine dipeptide at the N terminus of the N-degron (Ubi-CL-mCherry-sfGFP) is targeted for degradation by the E3 ubiquitin-protein ligase Doa10 with the E2 enzymes Ubc6/Ubc7 (ref. 33) (**Fig. 5b**). The Ubi-P-mCherry-sfGFP construct was included for comparison. Removal of N-terminal ubiquitin from Ubi-P-mCherry-sfGFP is inefficient and full-length Ubi-P-mCherry-sfGFP is not recognized by Ubr1 or Doa1 but is rapidly degraded by the ubiquitin-fusion degradation (UFD) pathway[33]. A nondegradable mCherry-sfGFP fusion served as a control (**Fig. 5b**). Each construct was introduced into a genome-wide library of yeast gene deletion mutants[35] using synthetic genetic array (SGA) technology[36] (**Fig. 5a**). Colonies of the obtained strains were imaged with a fluorescence plate reader, which provides robust, high-throughput measurements of whole-colony fluorescence intensities (**Supplementary Fig. 11**). Each screen was done in triplicate to control for experimental errors in the synthetic genetic array procedure and variability in colony size. To compensate for effects of gene deletions unrelated to protein turnover, we

calculated the differences (Δ-scores, **Fig. 5a**) between fluorescence measurements (the normalized sfGFP intensity and the mCherry/sfGFP intensity ratio) for each colony and corresponding values from a control screen performed with the nondegradable mCherry-sfGFP fusion (**Supplementary Fig. 12** and **Supplementary Note 6**). Strains with impaired degradation of a particular construct were identified by their high Δ-scores both for the mCherry/sfGFP intensity ratio, indicating increased stability, and for the sfGFP intensity, indicating increased abundance.

We reproducibly identified all known components of the *UBR1* branch in screens with Ubi-K/W/N/Q-mCherry-sfGFP constructs. For instance, the screens yielded the Nta1 amidase and the Ate1 arginyl-tRNA-protein transferase specifically required for degradation of constructs with N-terminal asparagine or glutamine residues[33] (**Fig. 5c**,**f**, **Supplementary Fig. 13**, **Supplementary Note 6** and **Supplementary Table 3**). The Ubi-CL-mCherry-sfGFP construct was stabilized in strains from which *DOA10* or *UBC7* were deleted, as expected[37] (**Fig. 5d**,**f** and **Supplementary Fig. 13**), whereas the *ubc6*Δ strain was not present in the library (but subsequently validated for its stabilizing effect; **Supplementary Fig. 14**). In addition, this screen identified *CUE1* as a new component of the *DOA10* branch of the N-end rule pathway (**Fig. 5d** and **Supplementary Fig. 14**). Cue1 recruits Ubc7 to the endoplasmic reticulum and the nuclear envelope, where Doa10 resides[38]. Significant stabilization of Ubi-CL-mCherry-sfGFP was reproducibly observed in deletion strains of various ubiquitin-proteasome system components and confirmed with cycloheximide chase experiments (**Fig. 5f**, **Supplementary Figs. 13** and **14**, **Supplementary Note 6** and **Supplementary Table 3**).

Ubi-P-mCherry-sfGFP was stabilized in strains lacking components of the UFD pathway, as expected (**Fig. 5e**). Deletions of several other ubiquitin-proteasome system components, including the ubiquitin-specific protease Ubp6, reproducibly stabilized Ubi-P-mCherry-sfGFP (**Fig. 5e**,**f**, **Supplementary Figs. 13** and **14**, **Supplementary Note 6** and **Supplementary Table 3**). Ubp6 removes ubiquitin chains from substrates at the proteasome and contributes to the regeneration of the free ubiquitin pool[39]. Accordingly, overexpression of ubiquitin partially restored the degradation of Ubi-P-mCherry-sfGFP in the *ubp6*Δ strain (**Supplementary Fig. 15**).

Ubr1 was recently shown to cooperate with Ufd4, the E3 enzyme of the UFD pathway, in ubiquitination of UFD substrates *in vitro*, but this cooperation could not be detected *in vivo*[40]. Using fluorescence imaging of whole colonies, we observed more stabilization of Ubi-P-mCherry-sfGFP in the *ufd4*Δ *ubr1*Δ strain compared to the *ufd4*Δ mutant (**Supplementary Fig. 16**). This demonstrates *in vivo* cooperation between Ubr1 and Ufd4 in the UFD pathway and suggests potential applications of tFTs to study cooperativity and redundancy of degradation pathways.

DISCUSSION

tFTs are versatile reporters that unify the study of protein turnover and trafficking in living cells from subcellular to population scales, thereby opening up new avenues for deciphering proteome homeostasis with high-throughput approaches. The modular nature of tFTs provides an opportunity to exploit state-of-the-art, single-color fluorescent proteins for sensitive measurements of intracellular dynamics. The bright mCherry-sfGFP timer allows measuring turnover, mobility and inheritance of endogenously expressed protein fusions in living cells on time scales from ~10 min to several hours. sfGFP can be fused with red fluorescent proteins with different maturation kinetics to generate a palette of tFTs suitable for studying processes on vastly different time scales, from a few minutes (e.g., transcriptional bursts) to several days (e.g., differentiation and morphogenesis). Established strategies for fluorescent protein evolution[41] can be used to broaden the spectrum of accessible time scales.

Notably, analysis of steady-state protein turnover with tFTs does not require time-course measurements. Using snapshot fluorescence imaging and automated yeast genetics, factors involved in degradation of specific proteins or components of individual degradation pathways can be readily identified with tFTs. Genome-wide protein tagging with tFTs should enable systematic characterization of proteome homeostasis across environmental and genetic perturbations. Standard approaches for genome manipulation with homologous recombination can be used for endogenous protein tagging in yeast[42]. High-throughput gene targeting is possible in mouse embryonic stem cells[43] and transcription activator-like effector nucleases are a promising tool for targeted genome editing in other model systems[44]. We anticipate the application of such technologies for systematic studies of protein dynamics with tFTs in whole organisms, thus minimizing artifacts commonly caused by ectopic expression of protein fusions[45].

Analysis of protein dynamics is key for understanding proteome homeostasis in health and disease. Many disorders, from infection to cancer, are associated with deficiencies in protein homeostasis[2–5]. tFTs should facilitate the investigation of cellular mechanisms of such diseases and allow the identification of clinically relevant compounds that modulate specific degradation pathways or affect the stability of critical proteins.

METHODS

Methods and any associated references are available in the online version of the paper.

Note: Supplementary information is available in the online version of the paper.

ACKNOWLEDGMENTS

We are grateful to Y. Belyaev, S. Terjung and the Advanced Light Microscopy Facility of EMBL for support with microscopy; A. Riddell, A.P. Gonzalez and the FACS Facility of EMBL for flow cytometry analyses; the CellNetworks cluster for funding to M.K., the German Research Foundation for funding to E.S. (SFB638), the Howard Hughes Medical Institute for funding to P.J.K., the European Molecular Biology Organization for funding to A.Kh. (EMBO ALTF 1124-2010), the EU-FP7 Network of Excellence in Systems Microscopy for funding to J.D.B. and W.H., and the Novartis Stiftung for funding to A.Ka. We thank P.I. Bastiaens, D. Gilmour and A. Kinkhabwala for discussions.

AUTHOR CONTRIBUTIONS

M.K. conceived and, together with E.S., A.Kh. and P.J.K., designed the project. A.Kh., M.M., A.B., A.Ka., S.T. and P.J.K. did all yeast experiments. B.R.M. did mammalian cell work. G.P. contributed reagents. P.J.K., J.D.B., A.Kh., W.H., M.W. and M.K. developed theory. P.J.K., J.D.B. and A.Kh. developed analytical tools. M.K., A.Kh. and P.J.K. wrote the manuscript with input from E.S. All authors discussed the results and commented on the manuscript.

COMPETING FINANCIAL INTERESTS

The authors declare no competing financial interests.

Published online at http://www.nature.com/doifinder/10.1038/nbt.2281.
Reprints and permissions information is available online at http://www.nature.com/reprints/index.html.

1. Schoenheimer, R. *The Dynamic State of Body Constituents* (Harvard University Press, Cambridge, MA, 1942).
2. Nakayama, K.I. & Nakayama, K. Ubiquitin ligases: cell-cycle control and cancer. *Nat. Rev. Cancer* **6**, 369–381 (2006).
3. Johnston, J.A., Ward, C.L. & Kopito, R.R. Aggresomes: a cellular response to misfolded proteins. *J. Cell Biol.* **143**, 1883–1898 (1998).
4. Morimoto, R.I. Proteotoxic stress and inducible chaperone networks in neurodegenerative disease and aging. *Genes Dev.* **22**, 1427–1438 (2008).
5. Balch, W.E., Morimoto, R.I., Dillin, A. & Kelly, J.W. Adapting proteostasis for disease intervention. *Science* **319**, 916–919 (2008).

6. Pratt, J.M. *et al.* Dynamics of protein turnover, a missing dimension in proteomics. *Mol. Cell. Proteomics* **1**, 579–591 (2002).
7. Eden, E. *et al.* Proteome half-life dynamics in living human cells. *Science* **331**, 764–768 (2011).
8. Zhang, L. *et al.* Method for real-time monitoring of protein degradation at the single cell level. *Biotechniques* **42**, 446–450 (2007).
9. Yen, H.-C.S., Xu, Q., Chou, D.M., Zhao, Z. & Elledge, S.J. Global protein stability profiling in mammalian cells. *Science* **322**, 918–923 (2008).
10. Gordon, A. *et al.* Single-cell quantification of molecules and rates using open-source microscope-based cytometry. *Nat. Methods* **4**, 175–181 (2007).
11. Yen, H.-C.S. & Elledge, S.J. Identification of SCF ubiquitin ligase substrates by global protein stability profiling. *Science* **322**, 923–929 (2008).
12. Newman, R.H., Fosbrink, M.D. & Zhang, J. Genetically encodable fluorescent biosensors for tracking signaling dynamics in living cells. *Chem. Rev.* **111**, 3614–3666 (2011).
13. Wu, B., Piatkevich, K.D., Lionnet, T., Singer, R.H. & Verkhusha, V.V. Modern fluorescent proteins and imaging technologies to study gene expression, nuclear localization, and dynamics. *Curr. Opin. Cell Biol.* **23**, 310–317 (2011).
14. Terskikh, A. *et al.* "Fluorescent timer": protein that changes color with time. *Science* **290**, 1585–1588 (2000).
15. Subach, F.V. *et al.* Monomeric fluorescent timers that change color from blue to red report on cellular trafficking. *Nat. Chem. Biol.* **5**, 118–126 (2009).
16. Tsuboi, T., Kitaguchi, T., Karasawa, S., Fukuda, M. & Miyawaki, A. Age-dependent preferential dense-core vesicle exocytosis in neuroendocrine cells revealed by newly developed monomeric fluorescent timer protein. *Mol. Biol. Cell* **21**, 87–94 (2010).
17. Merzlyak, E.M. *et al.* Bright monomeric red fluorescent protein with an extended fluorescence lifetime. *Nat. Methods* **4**, 555–557 (2007).
18. Pédelacq, J.-D., Cabantous, S., Tran, T., Terwilliger, T.C. & Waldo, G.S. Engineering and characterization of a superfolder green fluorescent protein. *Nat. Biotechnol.* **24**, 79–88 (2006).
19. Pereira, G., Tanaka, T.U., Nasmyth, K. & Schiebel, E. Modes of spindle pole body inheritance and segregation of the Bfa1p-Bub2p checkpoint protein complex. *EMBO J.* **20**, 6359–6370 (2001).
20. Malínská, K., Malínský, J., Opekarová, M. & Tanner, W. Visualization of protein compartmentation within the plasma membrane of living yeast cells. *Mol. Biol. Cell* **14**, 4427–4436 (2003).
21. Takizawa, P.A., DeRisi, J.L., Wilhelm, J.E. & Vale, R.D. Plasma membrane compartmentalization in yeast by messenger RNA transport and a septin diffusion barrier. *Science* **290**, 341–344 (2000).
22. Chen, T. *et al.* Multigenerational cortical inheritance of the Rax2 protein in orienting polarity and division in yeast. *Science* **290**, 1975–1978 (2000).
23. Strambio-De-Castillia, C., Niepel, M. & Rout, M.P. The nuclear pore complex: bridging nuclear transport and gene regulation. *Nat. Rev. Mol. Cell Biol.* **11**, 490–501 (2010).
24. D'Angelo, M.A., Raices, M., Panowski, S.H. & Hetzer, M.W. Age-dependent deterioration of nuclear pore complexes causes a loss of nuclear integrity in postmitotic cells. *Cell* **136**, 284–295 (2009).
25. Zabel, U. *et al.* Nic96p is required for nuclear pore formation and functionally interacts with a novel nucleoporin, Nup188p. *J. Cell Biol.* **133**, 1141–1152 (1996).
26. Makio, T. *et al.* The nucleoporins Nup170p and Nup157p are essential for nuclear pore complex assembly. *J. Cell Biol.* **185**, 459–473 (2009).
27. Steinkraus, K.A., Kaeberlein, M. & Kennedy, B.K. Replicative aging in yeast: the means to the end. *Annu. Rev. Cell Dev. Biol.* **24**, 29–54 (2008).
28. Winey, M., Yarar, D., Giddings, T.H. & Mastronarde, D.N. Nuclear pore complex number and distribution throughout the *Saccharomyces cerevisiae* cell cycle by three-dimensional reconstruction from electron micrographs of nuclear envelopes. *Mol. Biol. Cell* **8**, 2119–2132 (1997).
29. Khmelinskii, A., Keller, P.J., Lorenz, H., Schiebel, E. & Knop, M. Segregation of yeast nuclear pores. *Nature* **466**, E1 (2010).
30. Campbell, R.E. *et al.* A monomeric red fluorescent protein. *Proc. Natl. Acad. Sci. USA* **99**, 7877–7882 (2002).
31. Verzijlbergen, K.F. *et al.* Recombination-induced tag exchange to track old and new proteins. *Proc. Natl. Acad. Sci. USA* **107**, 64–68 (2010).
32. Ouellet, J. & Barral, Y. Organelle segregation during mitosis: Lessons from asymmetrically dividing cells. *J. Cell Biol.* **196**, 305–313 (2012).
33. Varshavsky, A. The N-end rule pathway and regulation by proteolysis. *Protein Sci.* **20**, 1298–1345 (2011).
34. Belle, A., Tanay, A., Bitincka, L., Shamir, R. & O'Shea, E.K. Quantification of protein half-lives in the budding yeast proteome. *Proc. Natl. Acad. Sci. USA* **103**, 13004–13009 (2006).
35. Winzeler, E.A. *et al.* Functional characterization of the *S. cerevisiae* genome by gene deletion and parallel analysis. *Science* **285**, 901–906 (1999).
36. Tong, A.H.Y. & Boone, C. High-throughput strain construction and systematic synthetic lethal screening in *Saccharomyces cerevisiae*. *Methods Microbiol.* **36**, 369–386 (2007).
37. Hwang, C.-S., Shemorry, A. & Varshavsky, A. N-terminal acetylation of cellular proteins creates specific degradation signals. *Science* **327**, 973–977 (2010).
38. Swanson, R., Locher, M. & Hochstrasser, M. A conserved ubiquitin ligase of the nuclear envelope/endoplasmic reticulum that functions in both ER-associated and Matalpha2 repressor degradation. *Genes Dev.* **15**, 2660–2674 (2001).
39. Leggett, D.S. *et al.* Multiple associated proteins regulate proteasome structure and function. *Mol. Cell* **10**, 495–507 (2002).
40. Hwang, C.-S., Shemorry, A., Auerbach, D. & Varshavsky, A. The N-end rule pathway is mediated by a complex of the RING-type Ubr1 and HECT-type Ufd4 ubiquitin ligases. *Nat. Cell Biol.* **12**, 1177–1185 (2010).
41. Shaner, N.C., Patterson, G.H. & Davidson, M.W. Advances in fluorescent protein technology. *J. Cell Sci.* **120**, 4247–4260 (2007).
42. Hardy, S., Legagneux, V., Audic, Y. & Paillard, L. Reverse genetics in eukaryotes. *Biol. Cell* **102**, 561–580 (2010).
43. Skarnes, W.C. *et al.* A conditional knockout resource for the genome-wide study of mouse gene function. *Nature* **474**, 337–342 (2011).
44. Bogdanove, A.J. & Voytas, D.F. TAL effectors: customizable proteins for DNA targeting. *Science* **333**, 1843–1846 (2011).
45. Yewdell, J.W., Lacsina, J.R., Rechsteiner, M.C. & Nicchitta, C.V. Out with the old, in with the new? Comparing methods for measuring protein degradation. *Cell Biol. Int.* **35**, 457–462 (2011).
46. Alber, F. *et al.* The molecular architecture of the nuclear pore complex. *Nature* **450**, 695–701 (2007).

ONLINE METHODS

Strain construction and growth conditions. Yeast strains used in this study are listed in **Supplementary Table 1**. Chromosomal gene tagging and gene deletion were done using standard procedures based on PCR targeting, as described[47]. Cassettes for PCR targeting were amplified with Phusion DNA polymerase (Finnzymes). Gene deletion and gene tagging were validated by PCR. Expression of protein fusions was validated using immunoblotting and confirmed with fluorescence microscopy, when appropriate.

Yeast strains were grown at 30 °C in SC-glucose medium (synthetic complete medium with 2% w/v glucose), unless indicated otherwise. Strains expressing mCherry-sfGFP fusions under the control of the *GAL1* promoter (**Fig. 4d**) were grown in SC medium with 3% w/v raffinose and 2% w/v galactose. For recombination-induced tag exchange (**Supplementary Fig. 6**), cells were grown in SC-glucose medium and incubated with 0.3 µg/ml β-estradiol (E8875, Sigma) for 3 h. To compare protein age between mother and bud compartments (**Figs. 2d** and **3c**), strains were synchronized in G1 (~2.5 h incubation with 10 µg/ml α-factor) to unequivocally distinguish mothers (with a mating projection or shmoo) from buds. Imaging was started 60 min after release from G1 arrest, as cells entered anaphase.

HeLa cells were cultured in DMEM medium with heat inactivated 10% FBS and 2 mM glutamine, in a humidified atmosphere with 5% CO_2 at 37 °C. 18 h before imaging, cells were transiently transfected with different mCherry-sfGFP constructs in 4-well chambers using Lipofectamine 2000 as described by the manufacturer (Invitrogen).

Plasmids and tagging cassettes. Plasmids used in this study are listed in **Supplementary Table 2**. Yeast codon-optimized sequences of mCherry[48] and sfGFP[18] were obtained by full gene synthesis. The monomeric V206R mutation[49] was introduced into the sequence of sfGFP. Cassettes for endogenous gene tagging with mCherry-sfGFP and sfGFP-mCherry by PCR targeting were designed to contain S2/S3 primer annealing sites compatible with previously described cassettes[47]. All Ubi-X-mCherry-sfGFP fusions are based on previously described Ubi-X-β-galactosidase and Ubi-XZ-Ura3 fusions[37,50].

A human codon-optimized mCherry-sfGFP sequence, generated by full-gene synthesis, was cloned into pCDNA5/FRT/TO (Invitrogen). This plasmid was used to construct Cyclin B-mCherry-sfGFP and CyclinB^{R42A}-mCherry-GFP expression vectors.

Flow cytometry. Yeast strains in the exponential growth phase were mixed with multi-spectral beads (3.0–3.4 µm Sphero Rainbow Calibration Particles (6 peaks), #556286, BD Biosciences) as an internal reference. Samples were measured in a Moflo cell sorter (Beckman Coulter). Argon and Krypton Sabre lasers (Coherent) were used for excitation of sfGFP (488 nm) and mCherry (568.2 nm), respectively. Fluorescence was detected with 512/15 and 630/40 bandpass filters for sfGFP and mCherry, respectively. 488 nm and 568 nm Holographic Notch filters placed in the optical path prevented detection of scattered laser light. BD FACSFlow was used as sheath fluid.

Populations of cells and reference beads were defined in raw data tables of each sample. Subsequent data standardization, correction and statistical analysis were performed in MATLAB (MathWorks). The fluorescence intensities of six species of reference beads in each sample were used to standardize cell intensity levels according to manufacturer's protocol, eliminating the influence of instrumental fluctuations on fluorescence intensity measurements. The standardized fluorescence intensities were background-corrected using autofluorescence of wild-type cells. mCherry/sfGFP intensity ratios of each sample were determined from median population intensities.

Fluorescence microscopy. Yeast strains were grown in SC-glucose medium at 30 °C and immobilized in glass bottom dishes (P35G-1.5-14-C, MatTek) or 8-well chambers (Lab-Tek 155409, Nunc) for 30 min before imaging. The dishes/chambers were coated for 5 min with 6% concanavalin A (C2010, Sigma) in water and excess concanavalin A was removed by washing with water. Imaging was done within 90 min after immobilization.

All images were recorded on a DeltaVision RT system (Applied Precision) consisting of an inverted epifluorescence microscope (IX70, Olympus) equipped with FITC and TRITC filters (Chroma Technology), a 100× NA 1.4 oil immersion objective (PlanApo, Olympus), a CoolSNAP HQ CCD camera (Photometrics), a motorized stage (NanoMotion II Control, Applied Precision) and a temperature-controlled chamber. Single-plane images (**Figs. 2d** and **3b**,**c** and **Supplementary Figs. 2**–**4** and **8**) or stacks spanning 5–6 µm with a step size of 300–400 nm (**Fig. 2a**–**c**,**e** and **Supplementary Figs. 5** and **6**) were acquired. Images of an empty position of the chamber (medium background), of wild-type cells (cellular background), of a uniformly fluorescent microscope slide (for flat field correction) and without illumination were acquired in each imaging session. The time-dependent intensity level of the light source was recorded during image acquisition using a sensor in the DeltaVision system.

Images were processed with custom software written in MATLAB (MathWorks). All images were corrected for background and for lamp intensity fluctuations. Wild-type cells were subjected to adaptive and iterative intensity thresholding to determine the levels of cellular autofluorescence. Cells expressing tagged nucleoporins were subjected to adaptive and iterative intensity thresholding to identify nucleoporin signals of whole cells and, separately, of nuclear envelope and cytoplasmic regions. Flat field correction was applied to the intensity levels in each segmentation mask. All measurements were subsequently corrected for cellular autofluorescence. The final intensity levels, their s.d., the resulting intensity ratio and the number of contributing pixels were stored for each segmented object. For the analysis of time-lapse induction series generated to determine the maturation kinetics of mCherry and sfGFP (**Supplementary Fig. 8a**), a module written in MATLAB (MathWorks) was used for cell tracking followed by manual track curation. Further details on the characterization of mCherry-sfGFP are provided in **Supplementary Methods**.

HeLa cells were imaged at 37 °C with a 60× NA 1.4 oil immersion objective (PlanApo, Olympus). Flat field and background corrections were applied to all images and mean fluorescence intensities of single cells or groups of contiguous cells were quantified using manual segmentation in ImageJ (National Institutes of Health, USA).

Constructs with mCherry-sfGFP fused to different degrons (**Fig. 5b**) were introduced into the SGA query strain Y8205 (ref. 36). Each resulting query strain was crossed in triplicate with a genome-wide library of diploid yeast strains with heterozygous gene deletions[35]. For replicates 2 and 3, strains with deletions of essentials genes were removed and the library was condensed to eliminate empty plate positions. The library was sporulated and the resulting spores were mated with the query strains using a RoToR pinning robot (Singer Instruments). All subsequent library manipulations—selection of diploids, sporulation, selection of haploids—were done using standard SGA protocols[36]. The resulting haploid strains each carrying an mCherry-sfGFP fusion and a specific gene deletion were grown in 1,536-colony format for 24–48 h before imaging.

The plates were imaged with a wide field IS4000MM-Pro fluorescence imager (Kodak) equipped with a 4-megapixel CCD camera and filters for sfGFP and mCherry fluorescence imaging (replicate 1) or with a wide field Decon imaging station (Decon Science Tec, Germany) equipped with an LED-based illumination system, a Retiga4000DC camera (QImaging) and filters for sfGFP (465/30 nm excitation, 520/35 nm emission) and mCherry (580/23 nm excitation, 628/40 nm emission) imaging (replicates 2 and 3). Images of a uniformly fluorescent plate were acquired for flat field correction. All sample images were flat field–corrected, segmented and the mean mCherry and sfGFP fluorescence intensities of each colony were extracted using the EBImage Bioconductor package[51]. Further data normalization and analysis were performed with the cellHTS2 Bioconductor package[52].

sfGFP fluorescence intensities and mCherry/sfGFP intensity ratios were corrected for plate edge effects with the B-score method[53], which was applied independently to the sfGFP and mCherry/sfGFP measurements. For comparison between different plates/screens, the corrected measurements were normalized by dividing by the per-plate median absolute deviation (MAD) of corrected measurements, yielding a normalized B-score $\hat{B}_{ijp}$ for each colony, where *i*, *j* and *p* reference the colony row, column and plate, respectively.

The normalized B-scores of all constructs were strongly affected in ~250 strains lacking genes mostly related to mitochondrial functions (**Supplementary Fig. 12**). These strains were identified in an automated fashion in the nondegradable control screen and omitted from the analysis.

A gene deletion was considered to stabilize an mCherry-sfGFP fusion in screen *s* if the respective colony showed increased sfGFP intensity and increased

mCherry/sfGFP intensity ratio, as compared to the corresponding colony in the control screen c (**Fig. 5a**). This comparison was quantified by the Δ-score ($\Delta^s_{ijp} = \hat{B}^s_{ijp} - \hat{B}^c_{ijp}$) calculated independently for the sfGFP and mCherry/sfGFP channels. Only gene deletions with Δ-score sfGFP > 0 (increased abundance) and Δ-score mCherry/sfGFP ratio > 0 (increased stability) were further examined (**Fig. 5c–f**). Gene deletions at a larger distance $d = \log(1 + M)$ from the center of the cloud of positive hits, where M is the Mahalanobis distance, were considered stronger hits. The natural logarithmic transformation was employed to obtain a reasonable spread in the scores for subsequent visualization, and an offset of unity was added to avoid negative scores.

Each screen replicate was analyzed independently. Gene deletions with $d \geq 6$ in at least one screen replicate were included in **Figure 5f**. A final d of each gene deletion was obtained by taking the median across replicates. All gene deletions with positive Δ-score sfGFP and Δ-score mCherry/sfGFP ratio are listed in **Supplementary Table 3**, ranked by the median d of the three screen replicates.

47. Janke, C. *et al.* A versatile toolbox for PCR-based tagging of yeast genes: new fluorescent proteins, more markers and promoter substitution cassettes. *Yeast* **21**, 947–962 (2004).
48. Shaner, N.C. *et al.* Improved monomeric red, orange and yellow fluorescent proteins derived from *Discosoma* sp. red fluorescent protein. *Nat. Biotechnol.* **22**, 1567–1572 (2004).
49. Zacharias, D.A., Violin, J.D., Newton, A.C. & Tsien, R.Y. Partitioning of lipid-modified monomeric GFPs into membrane microdomains of live cells. *Science* **296**, 913–916 (2002).
50. Bachmair, A., Finley, D. & Varshavsky, A. *In vivo* half-life of a protein is a function of its amino-terminal residue. *Science* **234**, 179–186 (1986).
51. Pau, G., Fuchs, F., Sklyar, O., Boutros, M. & Huber, W. EBImage–an R package for image processing with applications to cellular phenotypes. *Bioinformatics* **26**, 979–981 (2010).
52. Boutros, M., Brás, L.P. & Huber, W. Analysis of cell-based RNAi screens. *Genome Biol.* **7**, R66 (2006).
53. Malo, N., Hanley, J.A., Cerquozzi, S., Pelletier, J. & Nadon, R. Statistical practice in high-throughput screening data analysis. *Nat. Biotechnol.* **24**, 167–175 (2006).

doi:10.1038/nbt.2281